

# Real Compton Scattering at High $p_\perp$

Alan M. Nathan

University of Illinois at Urbana-Champaign

(for the E97-108 collaboration)

Contribution to Jefferson Lab Workshop on  
Physics & Instrumentation with 6-12 GeV Beams

Compton scattering ( $\gamma + p \rightarrow \gamma + p$ ) in the hard scattering limit is a potentially powerful probe of the short-distance structure of the nucleon. It is a natural complement to high  $Q^2$  exclusive reactions, such as elastic form factors and deeply virtual Compton scattering (DVCS), where the common feature is a hard energy scale, leading to a factorization of the transition amplitude into a part involving the overlap of soft (nonperturbative) wave functions and a perturbative hard scattering amplitude (HSA). For Real Compton Scattering (RCS), the hard scale is achieved when both  $s$  and the transverse momentum transfer  $p_\perp$  are large, and under these conditions RCS is sometimes referred to as “Wide-Angle Compton Scattering.” There are two types of questions that are interesting to investigate:

1. What is the appropriate mechanism for the HSA?
2. What can RCS teach us about the proton wave function?

In this report, we discuss the physics motivation for such measurements in light of these two questions. We then discuss some of the experimental considerations for a program at an upgraded JLab facility. Measurements up to 6 GeV are already in the planning stage (E97-108) [1].

Different HSA mechanisms can be distinguished by the manner in which  $p_\perp$  is shared among the constituents. Asymptotically this sharing is expected to occur in the HSA via hard gluon exchange (Fig. 1a), leading to the quark counting rule and scaling [2],

$$d\sigma/dt = \frac{f(\theta_{cm})}{s^n}, \quad (1)$$

where  $n=6$  for RCS. With modest precision, existing data from Cornell [3] approximately support scaling with  $n=6$  (see Fig. 2a). Nevertheless, Radyushkin [4] and others argue that this mechanism, when combined with realistic wave functions, badly underpredicts the RCS cross section. Instead he suggests that the dominant mechanism at experimentally accessible energies for both form factors and RCS is the handbag diagram (Fig. 1b,c), whereby the large  $p_\perp$  is absorbed on a single quark and shared by the overlap of high momentum components in the soft wave function. The latter are described in terms of the same nonforward parton densities (NFPD) that appear in deep inelastic scattering and DVCS, thereby offering the possibility of a unified description of all these processes. The dominance of the handbag diagram leads to the approximate factorization of the RCS cross section into the product of the Klein-Nishina (KN) cross section and a form factor-like object:

$$\frac{d\sigma}{dt} \approx \left( \frac{d\sigma}{dt} \right)_{\text{KN}} |F_{\gamma\gamma}(t)|^2 \quad F_{\gamma\gamma}(t) = \sum_f e_f^2 \int_0^1 F_f(x, t) \frac{dx}{x}, \quad (2)$$

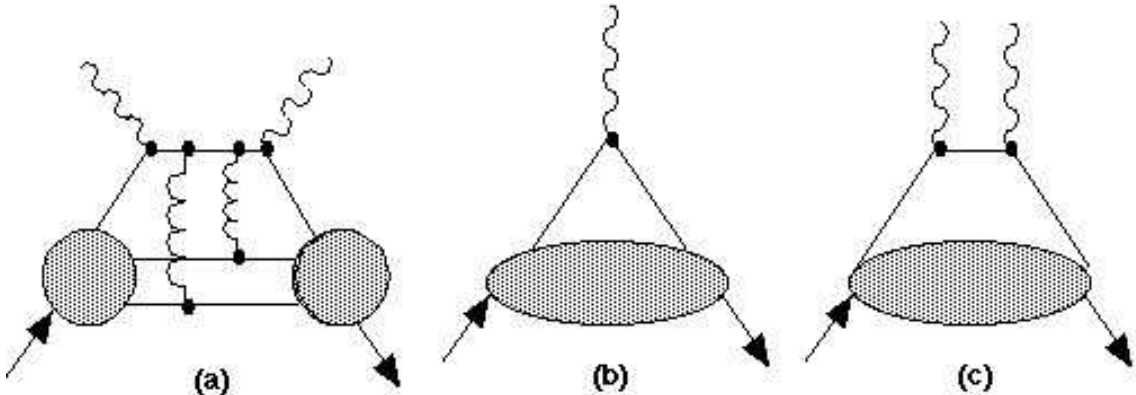


FIG. 1. Two-gluon exchange diagram for RCS (a) and handbag diagram for form factors (b) and RCS (c).

where the function  $F_f(x, t)$  is a particular projection of the NFPD for quark flavor  $f$ . This factorization leads to interesting consequences that can be tested experimentally. First, the scaling parameter  $n$  in Eq. 1 is angle dependent, as shown in Fig. 2a. Moreover the ratio  $\sigma/\sigma_{KN}$  is  $s$ -independent at fixed  $t$ , in approximate accord with the data (Fig. 2b). Further, the ratio yields  $F_{\gamma\gamma}(t)$ , which is a new form factor about which we know very little experimentally and which contains the interesting physics about the soft wave function. It is similar to but different from the Pauli form factor  $F_1(t)$  measured in elastic electron scattering:

$$F_1(t) = \sum_f e_f \int_0^1 F_f(x, t) dx.$$

For example,  $F_{\gamma\gamma}(t)$  is enhanced relative to  $F_1(t)$  due to the  $1/x$  weighting in the integral. Moreover, the weighting by the square of the quark charge means that  $F_{\gamma\gamma}(t)$  is sensitive to the flavor structure of the proton in a different way from  $F_1(t)$ , thereby providing another possible tool (along with parity-violating electron scattering) for decomposing the flavor structure. In particular, RCS is dominated by the  $u$ -quark distribution.

We now give some brief remarks about measurement with circularly polarized incident photons and a polarized proton target. The same physics is probed with an unpolarized target and measurement of the recoil polarization. In the absence of theoretical work in this area, we use the polarization-dependent KN cross section for guidance, for which the beam asymmetry

$$S_z \equiv \frac{\sigma(j = 1/2) - \sigma(j = 3/2)}{\sigma(j = 1/2) + \sigma(j = 3/2)} \quad (3)$$

is large (e.g.,  $\sim 0.7$  at  $E=6$  GeV and  $\theta_{cm}=90^\circ$ ). This suggests that polarized photons selectively scatter from quarks polarized in the opposite direction from the photon. Thus we have the exciting possibility that polarized RCS is sensitive to the spin-flavor structure of the generalized form factor, especially for the valence  $u$  quarks. Because of luminosity limitations with a polarized target or the small figure-of-merit with focal-plane polarimeters, these double-polarization experiments are only feasible when the scattering cross sections are large, i.e. for  $s < 8$  and  $-t < 4$  GeV $^2$ .

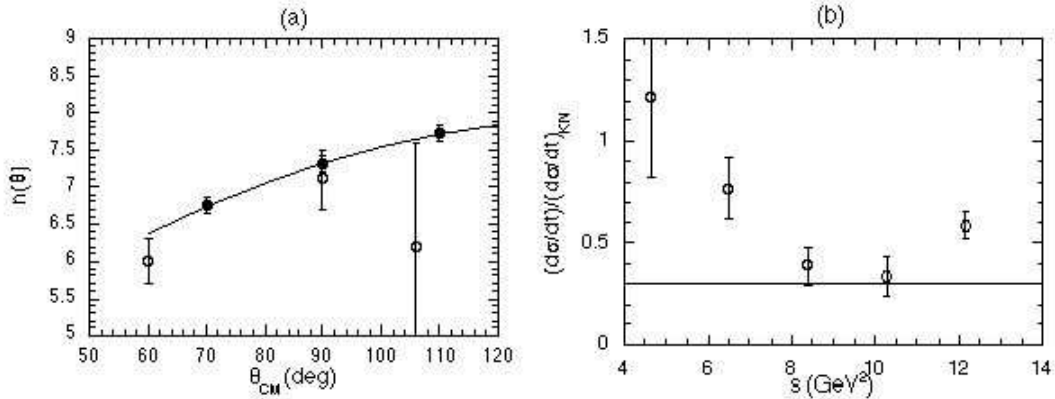


FIG. 2. (a) Scaling of RCS cross section at fixed  $\theta_{cm}$ . The open points are the Cornell data and the closed points are the projected results from E97-108. The curve is the prediction of Radyushkin, assuming dominance of the handbag diagram. (b) Ratio of the Cornell cross section to KN at fixed  $t = -2.45 \text{ GeV}^2$ . The horizontal line is the prediction of Radyushkin based on a model for the form factor and shows the level of agreement with the existing data.

Experimentally, one would like to test our understanding of the HSA mechanism by measuring RCS cross sections with good precision over a broad range of  $s$  and  $t$  in order to check the scaling behavior at both fixed  $\theta_{cm}$  and fixed  $t$ . Moreover, one would like to measure  $F_{\gamma\gamma}(t)$  over a similar range as  $F_1(t)$ . In Fig. 3a we show the kinematics appropriate to a 12 GeV upgrade of JLab, as well as limitations imposed by existing magnetic spectrometers and by the hard scattering condition  $p_\perp \geq 1 \text{ GeV}$ . The dots show the proposed kinematics for E97-108, for which the maximum incident energy is 6 GeV. We note that the only relevant data [3] extend up to  $s=12$ ,  $-t=6 \text{ GeV}^2$  but are of poor quality above  $s=8$ .

An overview of the experimental apparatus for RCS is shown in Fig. 3b. The small cross sections require high luminosity, which precludes the use of tagged photons for precision measurements. Instead a high intensity ( $\geq 10 \mu\text{A}$ ) beam of electrons impinges on a 6% copper radiator, and the *mixed* electron-photon beam is incident on a 15-cm  $\text{LH}_2$  scattering target. For incident photons near the bremsstrahlung endpoint, the recoil proton and scattered photon are detected with high angular precision in a magnetic spectrometer and photon spectrometer, respectively. An essential feature is to use the kinematic correlation between the scattered photon and recoil proton in the  $p(\gamma, \gamma'p)$  reaction to reduce the copious background of photons from the decay of  $\pi^0$ 's from the  $p(\gamma, \pi^0p)$  reaction, thereby placing stringent demands on the angular resolution of each spectrometer.

The photon spectrometer for E97-108 is currently being designed, but the important components have already been identified. First one needs a large-area segmented calorimeter with modest energy resolution and excellent position resolution. An array of 625 Pb-Glass blocks will be used, each with dimensions  $4 \times 4 \times 40 \text{ cm}^3$  and with an expected position resolution of order 5 mm. Next, electrons from  $ep$  scattering are deflected by a magnet and identified in a scintillator hodoscope, effectively removing this source of background. The

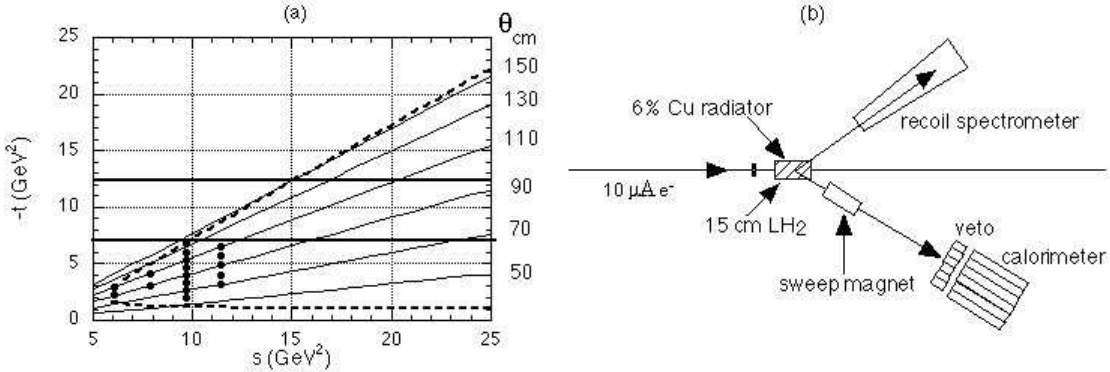


FIG. 3. (a) Kinematics of RCS measurements up to 12 GeV. The solid diagonal lines are contours at fixed  $\theta_{cm}$ ; the dashed diagonal lines indicate the upper and lower angular limits for  $p_{\perp} \geq 1$  GeV; the bold horizontal lines indicate the upper limit of the existing Hall A (4.5 GeV/c) and Hall C (7.5 GeV/c) spectrometers for the recoil proton. The dots are the proposed kinematics of E97-108. (b) Plan view of a possible RCS setup.

magnet also serves to sweep away low-energy electrons, thereby reducing the total energy flux on the detector. Finally a MWPC in front of the calorimeter will be used in a separate *in situ* calibration experiment to measure the position resolution of the calorimeter using  $ep$  electrons. The entire spectrometer will be mounted on a mechanical assembly that will allow changes in both scattering angle and radial distance, the latter needed to match the photon acceptance to that of the proton at different kinematic settings.

In summary, there is much exciting physics to be learned from RCS at high  $p_{\perp}$ . The general technique described here for E97-108 should work with only minor changes at an upgraded JLab facility, with event rates ranging from a few thousand/hour at 3 GeV to a few hundred/hour at 5 GeV to about 10/hour at 12 GeV. One can therefore look forward to a vigorous program at JLab extending well into the next decade.

## References

1. C. Hyde-Wright, A. M. Nathan, and B. Wojtsekhowski (co-spokespersons), JLab Proposal E97-108 (1997).
2. S. J. Brodsky and G. Farrar, Phys. Rev. Lett. **31**, 1953 (1973).
3. M. A. Shupe *et al.*, Phys. Rev. D **19**, 1929 (1979).
4. A. Radyushkin, hep-ph/9803316 (1998).